Yongkang Liu, Zongmei Yin, Junting Luo*, Zhang Chunxiang and Yanshu Zhang

The Constitutive Relationship and Processing Map of Hot Deformation in A100 steel

DOI 10.1515/htmp-2014-0182
Received October 10, 2014; accepted March 26, 2015

Abstract: Isothermal compression tests were conducted on A100 steel using a Gleeble 1500 thermal simulator at a temperature range of 900–1,200°C and strain rate range of 0.001–3 s^{-1}. Results show that the A100 steel has higher strength than the Aermet 100 steel at high temperatures. Constant values, such as A, α, and n, and activate energy Q were obtained through the regression processing of the stress–strain data curves under different strains. A set of constitutive equations for A100 steel was proposed by using an Arrhenius-type equation. The optimum processing craft ranges for A100 steel based on the analysis of the hot working diagram and deformation mechanism are as follows: temperature range of 1,000–1,100°C and strain rate range of 0.01–0.1 s^{-1}. The average grain size within this working range is 7–22.5 μm.

Keywords: A100 steel, the constitutive equations, compression tests, hot processing map

Introduction

A100 steel is a type of ultra-high-strength steel that uses C, Cr, and Mo as its strengthening elements. Its main components are 23Co13Ni11Cr3Mo. Based on the US patent, its performance is similar to that of the US-made Aermet 100 steel [1]. A100 steel has exceptional ductility and toughness and has excellent resistance to stress corrosion cracking and fatigue. Therefore, it has been mainly used to fabricate the critical mechanical parts of airplanes, such as the gear and the shaft gas turbine engine. Given the poor environment of these parts working, their performance requirements for service are high. A100 steel is generally subjected to high-temperature plastic forming to improve the microstructure morphology and streamline state and to meet the high-performance requirements [2, 3]. The constitutive equation can be the rheological characterization of material flow stress response to thermal parameters, such as deformation temperature, strain rate, and true strain [4]. Therefore, this approach is one of the important foundations for the process design and control of thermal deformation. To date, many studies have focused on the constitutive feature of Aermet 100 steel [5–7]. Research on Aermet 100 steel is relatively mature, but this US grade steel is different from A100 steel made in China in terms of mechanical performance [8–13]. Zhong examined the effect of isothermal tempering on microstructure and mechanical properties of ultrahigh strength A100 steel [14]. Tang et al. investigated the corrosion behaviour of the chromium plating on A100 steel under the outdoor exposure environments. There are few studies about the constitutive feature of A100 steel [15]. Therefore, the constitutive relations of thermal deformation in A100 steel should be established.

The constitutive equation describing the high-temperature flow stress and hot working diagram is established based on the hot compression test data of A100 steel. The optimum temperature and strain rate range of A100 steel thermal processing is acquired through a microstructure analysis, which provides the basis for the design and control of the deformation process for A100 steel.

Experimental materials and methods

The main chemical compositions of as-received A100 alloy are shown in Table 1. The A100 steel cylindrical specimens were machined to obtain the dimensions of 8 mm × 12 mm for the uniaxial compression tests. A shallow groove of Φ7.6 mm × 0.2 mm on the sample face was used to store lubricant to lower the friction

***Corresponding author: Junting Luo,** Education Ministry Key Laboratory of Advanced Forging & Stamping Technology and Science, Yanshan University, Qinhuangdao, Hebei, 066004, China; State Key Laboratory of Metastable Materials Science & Technology, Yanshan University, Qinhuangdao, Hebei, 066004, China, E-mail: zzymhylove@163.com
Yongkang Liu, Zongmei Yin, Education Ministry Key Laboratory of Advanced Forging & Stamping Technology and Science, Yanshan University, China
Zhang Chunxiang, State Key Laboratory of Metastable Materials Science & Technology, Yanshan University, China
Yanshu Zhang, Advanced Manufacture Technology Center, Beijing, China

Table 1: The main chemical compositions of the A100 steel.

Elements	C	Co	Ni	Cr	Mo
Mass fraction, %	0.23	13.85	11.73	3.13	1.25

between the anvil and the specimen interface. Isothermal compression was conducted in a Gleeble 1500 thermal simulator at constant strain rates of 0.001, 0.01, 0.1, 1.0, and 3.0 s^{-1} and at experimental temperatures of 900–1,200°C with 50°C intervals. Before the hot compression, the specimens were heated to 1,200°C at a speed of 20°C/s, with heat preservation for 5 min, and cooled to the deformation temperature of 10°C/s, with heat preservation for 10 min. The specimens were water-quenched after deformation to maintain the deformed microstructure.

Results and discussion

Stress–strain curves and deformation mechanism analysis

The curves of the relationship between flow stress and strain in A100 steel under different temperatures and strain rates are shown in Figure 1. Stress rapidly increases with the strain increase at the beginning of the deformation and then gradually decreases after reaching its peak. The flow stress then reaches a steady state when it reaches a certain true strain. With the true strain larger than 0.8, the degree of strain hardening is higher than the degree of dynamic recrystallization and dynamic recovery softening. The stress, in turn, shows an increasing trend, and a secondary hardening phenomenon is observed. The earlier peak of the

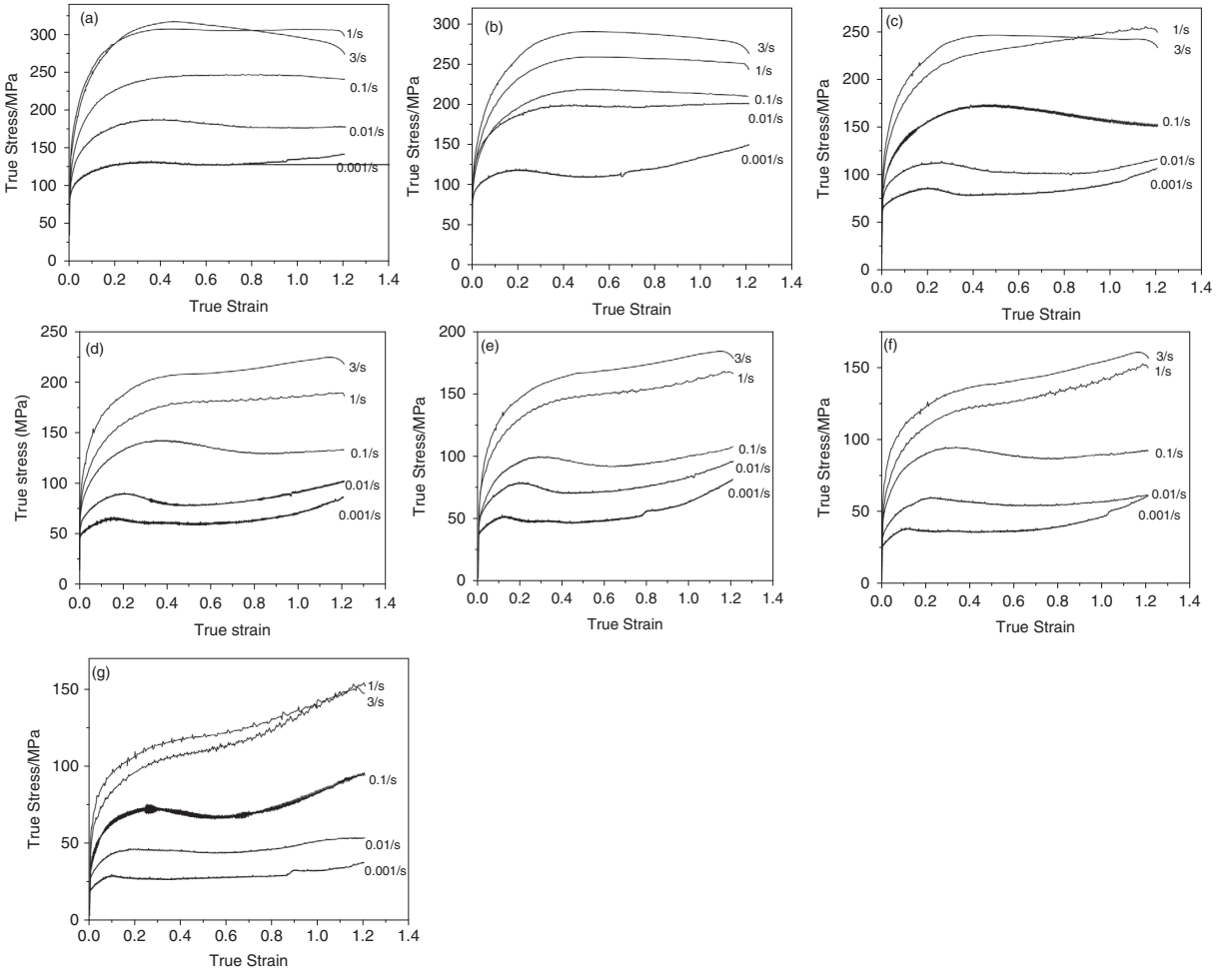

Figure 1: The stress–strain curve under different testing conditions: (a) 900°C; (b) 950°C; (c) 1,000°C; (d) 1,050°C; (e) 1,100°C; (f) 1,150°C; (g) 1,200°C.

stress appears with the temperature increase, and the stress gradually stabilizes with the deformation increase. Table 2 shows the flow stress under different deformation conditions of A100 steel, and Table 3 shows the flow stress values under different deformation conditions of Aermet 100 steel. Comparing these tables it is seen that A100 steel has higher temperature flow stress values than Aermet 100 steel and that the high-temperature strength of A100 steel is more superior to that of Aermet 100 steel.

The microstructure grain sizes under different deformation conditions of A100 steel are shown in Figure 2 and Table 4. Dynamic recrystallization occurred at 900°C with a strain rate of 0.001 s^{-1}. The softening mechanisms used were dynamic recrystallization and dynamic recovery. The microstructure forged organizations at 900°C and strain rate of 1 s^{-1}. As the dynamic recrystallization grains were small, the softening mechanism used was dynamic recovery. The recrystallization volume fraction was 80%, and the average grain size was approximately 10 μm when the temperature was 1,000°C and strain rate was 1 s^{-1}. Complete recrystallization occurred at 1,100°C, strain rate of 1 s^{-1}, and average grain size of approximately 15 μm. The average grain size increased with the decreasing strain rate because the final strain of isothermal compression tests is the same, the deformation time becomes longer with the decreasing strain rate, and the deformation time becomes longer in favour of recrystallization. The grain growth trend was clear at a temperature range of 1,000–1,100°C and strain rate of 0.001 s^{-1}. Grain growth was also clear when the temperature was higher than 1,150°C.

Deformation constitutive equations

The flow stress σ of A100 steel in hot compressive deformation is related to temperature T and strain rate $\dot{\varepsilon}$. The hyperbolic sine constitutive equation of A100

Table 2: Flow stress value of A100 under different deformation conditions.

Strain	Strain rate (s^{-1})	Temperature (°C)						
		900	950	1,000	1,050	1,100	1,150	1,200
0.8	0.001	129.41	120.02	83.857	56.231	39.481	28.457	63.183
	0.01	177.24	197.62	101.61	83.846	76.321	55.005	45.861
	0.1	246.38	215.17	163.28	129.36	94.634	86.879	71.948
	1	305.55	256.19	241.56	181.81	153.82	133.74	123.24
	3	305.68	286.38	244.38	213.32	173.54	146.57	130.37
0.9	0.001	131.6	126.12	86.903	58.717	42.454	32.245	67.417
	0.01	176.9	198.02	102.41	87.661	79.85	55.851	47.984
	0.1	246.13	214.4	159.44	129.19	97.089	88.149	76.321
	1	305.63	255.19	245.13	183.61	156.27	138.47	130.63
	3	301.1	284.14	243.32	216.48	176.64	150.23	135.27

Table 3: Flow stress value of Aermet 100 under different deformation conditions.

Strain	Strain rate (s^{-1})	Temperature (°C)					
		800	900	1,000	1,100	1,150	1,200
0.8	0.01	179.656	117.336	65.392	35.121	31.176	26.114
	0.1	248.346	175.748	100.639	55.237	45.780	42.546
	1	271.553	226.251	151.005	93.362	77.565	61.541
	10	279.521	214.932	169.097	116.118	103.078	81.220
0.9	0.01	180.01	122.98	69.324	33.882	31.321	27.506
	0.1	258.03	180.01	101.32	58.641	46.265	44.433
	1	284.66	231.40	153.38	93.299	77.99	62.311
	10	279.04	210.18	153.38	115.52	104.55	82.702

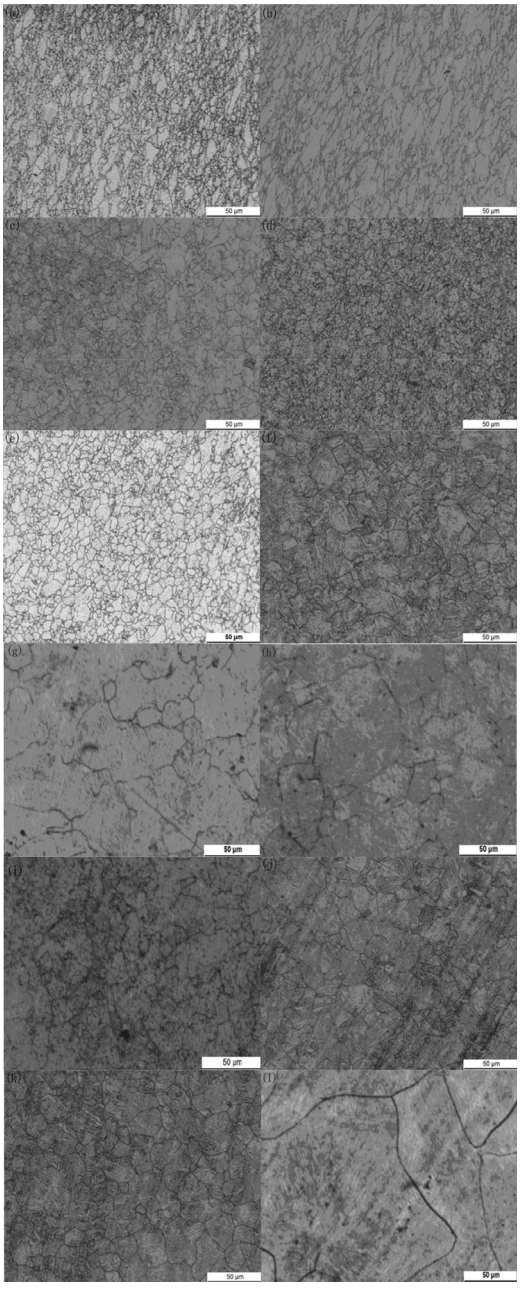

Figure 2: Microstructure of A-100 steel under different testing conditions: (a) 900°C–0.01 s^{-1}; (b) 900°C–1 s^{-1}; (c) 1,000°C –0.01 s^{-1}; (d) 1,100°C–0.1 s^{-1}; (e) 1,000°C–1 s^{-1}; (f) 1,100°C–1 s^{-1}; (g) 1,050°C–0.001 s^{-1}; (h) 1,100°C–0.001 s^{-1}; (i) 1,100°C–0.01 s^{-1}; (j) 1,100°C–0.1 s^{-1}; (k) 1,150°C–1 s^{-1}; (l) 1,200°C–0.001 s^{-1}.

steel is expressed as follows based on the work of Sellars [16]:

$$\dot{\varepsilon} = A[\sinh(\alpha\sigma)]^n \exp(-Q/RT) \quad (1)$$

where A, α, n are material constants, $\dot{\varepsilon}$ is the strain rate (s^{-1}), σ is the flow stress (MPa), Q is the activation energy of deformation (kJ/mol), R is the gas constant

Table 4: Grain size under different deformation conditions (μm).

Strain rates (s^{-1})	Temperature (°C)						
	900	950	1,000	1,050	1,100	1,150	1,200
0.001	7.9	10	15.3	51.0	59.7	70.7	97.4
0.01	8.3	7.1	11.6	22.3	20.9	36.4	52.8
0.1	6.3	8.2	7.9	13.8	21.1	25.1	26.1
1	7.7	8.5	6.9	9.4	14.7	17.6	24.4
3	5.4	7.6	10.2	7.9	18.5	21.4	17.9

($R = 8.31\ \mathrm{J/(mol \cdot K)}$), and T is the absolute deformation temperature (K).

Material constants A, α, n, and Q were found to be functions of strain [17]. The three material constants evaluated at strains of 0.1–1.2 with an interval of 0.1 were plotted and fitted using polynomial equations and power equations. With the true strain of 0.1 as an example, the specific fitting process is as follows:

In Figure 3(a) and (b) are the relation curves of $\ln\dot{\varepsilon}$ / $\ln\sigma$ and $\ln\dot{\varepsilon}/\sigma$ at the strain value of 0.1, respectively. The average value of the straight line slope in Figure 3(a) is n1. Therefore, the average value of all the straight line slopes in Figure 3(b) is $\alpha = \beta/\mathrm{n}_1 = 0.0102$.

Taking the logarithm on both sides of eq. (1), the following equation can be obtained:

$$\ln\ A + n\ln\sinh(\alpha\sigma) = \ln\dot{\varepsilon} + Q/RT \quad (2)$$

where α is substituted into eq. (2). The relationship curves of $\ln\dot{\varepsilon}$ and $\ln(\sinh(\alpha\sigma))$ under the temperature and strain rate can then be obtained (Figure 3(c)). The average slope of the relationship curves is $n = 5.947886$.

Taking the partial differential on both sides of eq. (1), the equation can obtain the activate energy Q as follows:

$$Q = R\left[\partial\ln\sinh(\alpha\sigma)/\partial(1/T)\right] \cdot \left[\partial\ln\dot{\varepsilon}/\partial\ln\sinh(\alpha\sigma)\right]_T \quad (3)$$

Under the condition of a constant strain rate, the Q value remains unchanged within a certain temperature range. Each slope of the linear fitting line of (1,000/T) and $\ln(\sinh(\alpha\sigma))$ can be calculated. The average slope figure is $\mathrm{s} = 10.4 \times 10^3$; n and s are substituted in eq. (3) to obtain the constant value of $Q = 513.795$ KJ/mol. Equation (2) shows that the intercept value of the $\ln(\sinh(\alpha\sigma)) - \ln\dot{\varepsilon}$ relation curve is the difference between $\ln A$ and (Q/RT). According to the above Q, R, T values under different temperatures, the A value can be obtained and the mean value is $A = 3.25 \times 10^{18}$. The relationship between A100 steel flow stress and strain rate at the true strain of 0.1 is as follows:

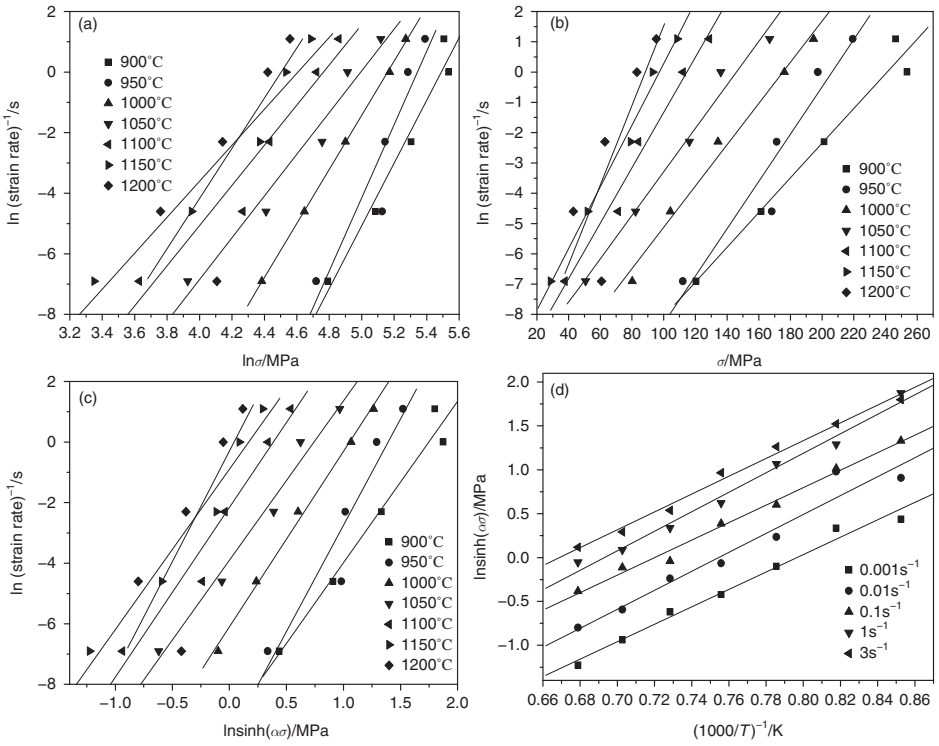

Figure 3: The fitting curve when the strain is 0.1. (a) The curves of relationship between $\ln\dot{\varepsilon}$ and $\ln\sigma$; (b) The curves of relationship between $\ln\dot{\varepsilon}$ and σ; (c) The curves of relationship between $\ln\dot{\varepsilon}$ and $\ln(\sinh(\alpha\sigma))$; (d) The curves of relationship between $(1{,}000/T)$ and $\ln(\sinh(\alpha\sigma))$.

$$\begin{aligned}\dot{\varepsilon} &= A[\sinh(\alpha\sigma)]^n \cdot \exp(-Q/RT)\\ &= 3.24736 \times 10^{18}[\sinh(0.010149\sigma)]^{5.947886}\\ &\quad \cdot \exp(-513,794.9/RT)\end{aligned} \tag{4}$$

A set of constitutive equations for A100 steel was proposed by using an Arrhenius-type equation. The fitted equations for the constants are functions of strain, as shown in eq. (5).

$$\begin{cases} Q = 392,938\varepsilon^{-0.116} (R^2 = 0.9878)\\ A = 8 \times 10^{13}\varepsilon^{-4.4294} (R^2 = 0.9802)\\ n = 42.138\varepsilon^6 - 152.24\varepsilon^5 + 217.27\varepsilon^4 - 159.58\varepsilon^3\\ \quad +69.649\varepsilon^2 - 19.448\varepsilon + 7.3312 (R^2 = 0.9993)\\ \alpha = -0.0734\varepsilon^6 + 0.2438\varepsilon^5 - 0.2898\varepsilon^4 0.1381\varepsilon^3\\ \quad -0.0124\varepsilon^2 - 0.0096\varepsilon + 0.0111 (R^2 = 0.9979)\end{cases} \tag{5}$$

Equation (5) represents the constitutive equations for A100 steel working at high temperatures. Equation (5) is then substituted into eq. (6) to obtain the calculation value of the flow stress.

$$\sigma = \frac{1}{\alpha}\ln\left\{\left(\frac{\dot{\varepsilon}}{A}\exp\left(\frac{Q}{RT}\right)\right)^{\frac{1}{n}} + \left[\left(\frac{\dot{\varepsilon}}{A}\exp\left(\frac{Q}{RT}\right)\right)^{\frac{2}{n}} + 1\right]^{\frac{1}{2}}\right\} \tag{6}$$

The results show that the agreement between the measured and calculated values is satisfactory. Therefore, the present constitutive equations are an effective approach to predict the load during the thermal operation of A100 steel.

Hot processing map

The non-steady-state range increases with the increasing deformation degree during the hot deformation process. The hardening phenomenon is serious when the strain is above 0.8. Therefore, the power dissipation and rheological instability figures when the strain is 0.8 are established to determine the thermal processing feasible region. Based on the stress–strain curves, the flow stress values at different temperatures and strain rates are obtained. At a certain temperature, the cubic spline $\ln\sigma - \ln\dot{\varepsilon}$ fitting curve is adopted by using eq. (7). The relation between the strain rate sensitivity index m at a certain temperature and the strain rate values is shown in eq. (8). The power dissipation efficiency factor η is calculated using eq. (9). The contour curve of the power dissipation efficiency factor is shown in Figure 4. The figure number on the contour line represents the values of the power dissipation efficiency factor η. Figure 4 shows that the power dissipation efficiency factor of A100 steel

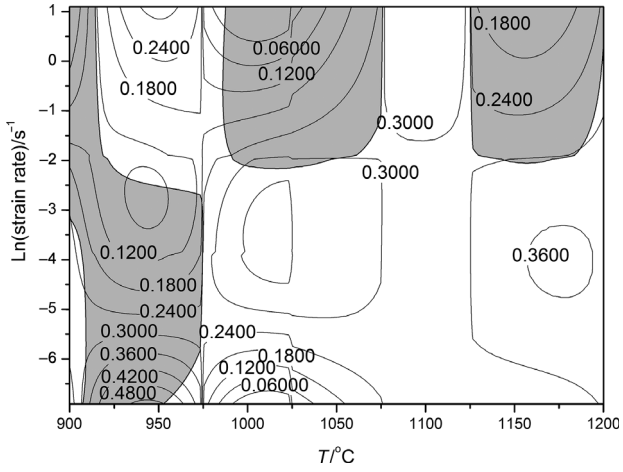

Figure 4: Power dissipation and rheological instability when the strain is 0.85.

is 5–42%. The dynamic energy consumption behaviour of A100 steel clearly varies with the deformation temperature and the strain rate. The η value increases gradually with the reduction in the rise of temperature and strain rate values. The calculation formula $\xi(\dot{\varepsilon})$ is shown in eq. (10). Plastic processing is unstable when $\xi(\dot{\varepsilon})<0$. The shaded areas in Figure 4 are the regions of $\xi(\dot{\varepsilon})<0$, which are thermal processing hazardous areas. The instability area for the steady-state rheological instability in the figure is mainly concentrated in the high-strain-rate zone and in the low-temperature and high-strain rate zone.

$$\ln\sigma = a(\ln\dot{\varepsilon})^3 + b(\ln\dot{\varepsilon})^2 + c\ln\dot{\varepsilon} + d \tag{7}$$

$$\frac{\partial\ln\sigma}{\partial\ln\dot{\varepsilon}} = 3a(\ln\dot{\varepsilon})^2 + 2b(\ln\dot{\varepsilon}) + c = m \tag{8}$$

$$\eta = J/J_{\max} = 2m/(m+1) \tag{9}$$

$$\xi(\dot{\varepsilon}) = \partial\ln\left(\frac{m}{m+1}\right)\Big/\partial\ln\dot{\varepsilon} + m \tag{10}$$

In terms of the integrated power dissipation and rheological instability of the figure, the dynamic recrystallization zone is preferred in hot working processes to avoid a flow instability region. This condition is due to the high efficiency of power dissipation, good mechanical performance, and easy control of the microstructure in the dynamic recrystallization zone. Figure 4 shows that the dissipation factor in the region with a temperature range of 1,000–1,200°C and a strain rate range of 0.001–0.14 s^{-1} is between 0.21 and 0.42. These values show that dynamic recrystallization is the main softening mechanism for this area. The dissipation factor for the region with a temperature range of 1,050–1,100°C and a strain rate range of 0.1–3 s^{-1} is between 0.24 and 0.27. Its main softening mechanisms are dynamic recrystallization and dynamic recovery. Therefore, the hot processing security zone of A100 steel consists of two parts: one for the temperature range of 1,000–1,200°C and the strain rate of 0.001–0.1 s^{-1}, and the other for the temperature range of 1,050–1,100°C and the strain rate of 0.1–3 s^{-1}. Given the microstructure analysis results in Table 4, the optimum processing craft range is 1,000–1,100°C and 0.01–0.1 s^{-1}. The average grain size within this working range is 7–22.5 μm, which meets the performance and grain size requirements for aviation forging.

Conclusions

1. The hot compression simulation experiments of A100 steel at a temperature range of 900–1,200°C and strain rate range of 0.001–3 s^{-1} show that A100 steel has higher strength than Aermet 100 steel at high temperatures.
2. The functions of material constants A, α, and n, and activate energy Q with respect to strain were obtained based on the Arrhenius equation. A set of constitutive equations for A100 steel was proposed by using an Arrhenius-type equation.
3. The hot processing map of A100 steel was established, and the optimum processing craft range for A100 steel was obtained as follows: temperature range of 1,000–1,100°C and strain rate range of 0.01–0.1 s^{-1}. The average grain size within this working range is between 7 and 22.5 μm.

Funding: This work was financially supported by National major projects–high-end CNC machine tools and basic manufacturing equipment (Grant 2012zx04010-081).

References

[1] R.M. Hemphill and D.E. Wert, High strength high fracture toughness alloy, US Patent: No. 328875, 1989.
[2] S.Q. Huang, Y.P. Yi and P.C. Li, Trans. Mater. Heat Treat., 24 (2013) 99–103.
[3] S.Q. Huang, Y.P. Yi and P. Li, J. Mater Res., 25 (2011) 283–288. (in Chinese).
[4] X.M. Zhang, F.Y. Cao, H.Y. Yue et al., Rare Metal Mater. Eng., 42 (2013) 937–941.

[5] G.L. Ji, F.G. Li, Q.H. Li, H.Q. Li and Z. Li, Mater. Sci. Eng. A, 527 (2010) 1165–1171.
[6] G.L. Ji, F.G. Li, Q.H. Li, H.Q. Li and Z. Li, Mater. Sci. Eng. A, 527 (2010) 2350–2355.
[7] L.C. Chhabildas and W.D. Reimhart, J. Phys., 110 (2003) 767–771.
[8] L.D. Wang, L.Z. Jiang and M. Zhu, J. Mater. Sci. Technol., 21 (2005) 710–714.
[9] M.B. Mohammed, C.J. Bennett, P.H. Shipway and T.H. Hyde, WIT Trans. Eng. Sci., 68 (2010) 253–265.
[10] S. Michael, P. Karen and Bray Simon, ASM Proceedings of the International Conference: Trends in Welding Research, Raleigh, NC, United states (2013), 1071–1078.
[11] C. Hao, L. Dong, T. Hai-bo, Z. Shu-quan, R. Xian-zhe and W. Hua-Ming, J. Iron Steel Res., 20 (2013) 79–84.
[12] K. Manigandan, T.S. Srivatsan, D. Tammana, B. Poorganji and V.K. Vasudevan, Mater. Sci. Eng. A, 601 (2014) 29–39.
[13] Q. Huijuan, Li Fuguo, Ji Guoliang and X. Meili, Rare Metal Mater. Eng., 43 (2014) 926–931.
[14] P. Zhong, J. Iron Steel Res. Int., 14 (2007) 292–295.
[15] Z.H. Tang et al., Mater Eng. 9 (2011) 50–55. (in Chinese).
[16] C.M. Sellars, Mater. Sci. Technol., 1 (1985) 325–328.
[17] Z. Zeng, S. Jonsson and Y. Zhang, Mater. Sci. Eng. A, 505 (2009) 116–119.